

Anomalous magnetic interference of cross-type Josephson junctions exposed to oblique magnetic fields

Yasunori Mawatari

National Institute of Advanced Industrial Science and Technology (AIST),
Tsukuba, Ibaraki 305–8568, Japan

Abstract. Gauge-invariant phase difference and critical currents of cross-type Josephson junctions with thin and narrow superconducting strips exposed to three-dimensional magnetic fields are theoretically investigated. When a sandwich-type Josephson junction in the xy plane is exposed to parallel magnetic fields H_x and H_y , the phase difference linearly depends on the spatial coordinates, x and y , and the critical currents exhibit the standard Fraunhofer-type magnetic interference. The perpendicular field H_z , on the other hand, nonlinearly modulates the distribution of the phase difference and the critical currents as the functions of the oblique field exhibit anomalous magnetic interference. We obtain simple analytical expressions for critical currents of small cross-type junctions by neglecting the effects of self-field and trapped vortices. The resulting dc critical currents show anomalous and diverse interference patterns depending on the parallel and perpendicular magnetic fields.

1. Introduction

One of the most fascinating behaviors of the static response of Josephson junctions is the interference patterns in the magnetic-field dependence of the dc critical current I_c . The I_c of small junctions exhibit Fraunhofer-type interference patterns [1, 2, 3], and the interference behavior in response to a magnetic flux in steps of the flux quantum $\phi_0 = h/2e = 2.07 \times 10^{-15}$ Wb is a key phenomenon for application to ultrasensitive magnetometers, superconducting quantum interference devices (SQUIDs) [2, 4, 5].

Anomalous magnetic interference in I_c of Josephson junctions has been extensively investigated by considering the effects of inhomogeneous current density in the junction [4, 6], trapped vortices [7, 8, 9, 10], local current injection [11, 12, 13], ferromagnetic π junctions [14, 15, 16], and semiconductor junctions [17]. Magnetic interference in I_c are also analyzed to investigate the edge states in topological insulators [18, 19, 20] and in graphene [21].

Here we demonstrate that anomalous interference patterns appear even in the naive case of sandwich-type Josephson junctions in *oblique* magnetic fields. Although the response of junctions to *parallel* magnetic fields is well understood [4], only a limited number of works have been published on the response to *perpendicular* and/or *oblique* magnetic fields [7, 22, 23, 24, 25]. The systematic response of dc critical current of Josephson junctions to *oblique* magnetic fields remains unclear.

In this paper, we theoretically investigate the dc critical current I_c of cross-type junctions in oblique magnetic fields. We derive simple analytical expressions for I_c as a function of the three-dimensional magnetic field $\mathbf{H} = (H_x, H_y, H_z)$ by assuming that the magnetic screening effect in small junctions is weak and that no vortices are trapped in the junctions. We demonstrate a variety of anomalous interference patterns in the field dependence of I_c , although the analytical formulae of I_c are quite simple.

This paper is organized as follows. The static two-dimensional distribution of the gauge-invariant phase difference in small sandwich-type Josephson junctions is considered in Sec. 2. Analytical expressions for I_c of cross-type Josephson junctions are derived and a variety of the interference patterns of I_c as functions of the parallel and perpendicular (i.e., in-plane and out-of-plane) magnetic fields are demonstrated in Sec. 3. Our results are summarized in Sec. 4.

2. Gauge-invariant phase difference

In this section we consider the static two-dimensional distribution of the gauge-invariant phase difference in sandwich-type Josephson junctions by neglecting the effects of self-field and trapped vortices.

2.1. Basic equations for two-dimensional Josephson junctions

We consider a Josephson junction as shown in figure 1 in which a barrier layer of thickness d_j is located at $|z| < d_j/2$ sandwiched between two superconducting layers.

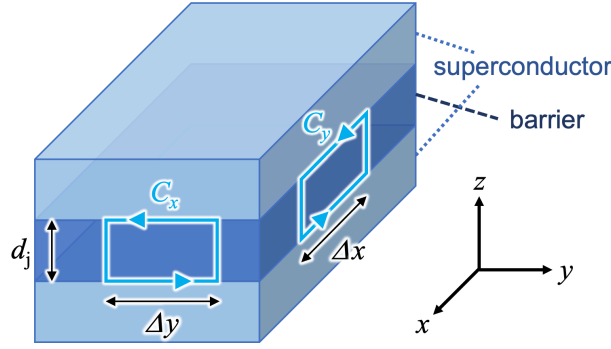


Figure 1. Schematic of the Josephson-junction structure in which a barrier layer of thickness d_j located at $|z| < d_j/2$ between superconducting layers at $|z| > d_j/2$. C_x and C_y are closed rectangular contours of $\Delta y \times d_j$ in the yz plane and of $\Delta x \times d_j$ in the zx plane, respectively.

The supercurrent density associated with the order parameter $\psi = |\psi| \exp(i\varphi)$ based on Ginzburg-Landau theory is given by [3, 4]

$$\mathbf{J} = \frac{1}{\mu_0 \lambda^2} \left(\frac{\phi_0}{2\pi} \nabla \varphi - \mathbf{A} \right), \quad (1)$$

where μ_0 is the vacuum permeability, λ is the London penetration depth, φ is the phase, and \mathbf{A} is the vector potential related to the magnetic induction $\mathbf{B} = \nabla \times \mathbf{A}$. We assume that suppression of $|\psi|$ from its equilibrium value is negligible.

The gauge-invariant phase difference $\theta(x, y)$ at the junction, which is associated with the phase $\varphi(x, y, z)$ and the z component of the vector potential $A_z(x, y, z)$, is defined by [3, 4, 26]

$$\theta(x, y) = \varphi(x, y, +d_j/2) - \varphi(x, y, -d_j/2) - \frac{2\pi}{\phi_0} \int_{-d_j/2}^{+d_j/2} A_z(x, y, z) dz. \quad (2)$$

We calculate the contour integral of the vector potential along the rectangular contour C_x which has vertices at $(x, y, \pm d_j/2)$ and $(x, y + \Delta y, \pm d_j/2)$ (figure 1). Using Stokes theorem, we have

$$\oint_{C_x} \mathbf{A} \cdot d\mathbf{s} = \int_y^{y+\Delta y} dy \int_{-d_j/2}^{+d_j/2} dz B_x = B_x d_j \Delta y. \quad (3)$$

for a thin junction layer $d_j \rightarrow 0$ and narrow contour width $\Delta y \rightarrow 0$. Using equations (1) and (2), we also obtain the following expression:

$$\begin{aligned} \oint_{C_x} \mathbf{A} \cdot d\mathbf{s} &= \left[-A_y(x, y, +d_j/2) + A_y(x, y, -d_j/2) \right] \Delta y + \int_{-d_j/2}^{+d_j/2} dz [A_z(x, y + \Delta y, z) - A_z(x, y, z)] \\ &= -\frac{\phi_0}{2\pi} \frac{\partial \theta(x, y)}{\partial y} \Delta y + \mu_0 \lambda^2 \left[J_y(x, y, +d_j/2) - J_y(x, y, -d_j/2) \right] \Delta y. \end{aligned} \quad (4)$$

Equations (3) and (4) yield [3, 4, 7, 27, 28]

$$\frac{\phi_0}{2\pi} \frac{\partial \theta(x, y)}{\partial y} = -B_x d_j + \mu_0 \lambda^2 \left[J_y(x, y, +d_j/2) - J_y(x, y, -d_j/2) \right]. \quad (5)$$

The contour integral along C_y of \mathbf{A} also yields a similar equation:

$$\frac{\phi_0}{2\pi} \frac{\partial \theta(x, y)}{\partial x} = +B_y d_j + \mu_0 \lambda^2 \left[J_x(x, y, +d_j/2) - J_x(x, y, -d_j/2) \right]. \quad (6)$$

2.2. Cross-type junctions with thin superconducting nanostrips

We now consider cross-type junctions with two superconducting nanostrips consisting of a top strip of thickness d_{s1} and width w_1 along the y axis and a bottom strip of thickness d_{s2} and width w_2 along the x axis, as shown in figure 2.

We assume that the thicknesses of the strips are smaller than the London penetration depth, $d_{s1} < \lambda$ and $d_{s2} < \lambda$, and the widths are smaller than the Pearl length, $w_1 < \lambda^2/d_{s1}$ and $w_2 < \lambda^2/d_{s2}$, such that magnetic screening is weak in the superconducting nanostrips. The current density in thin and narrow superconducting strips is simply obtained by

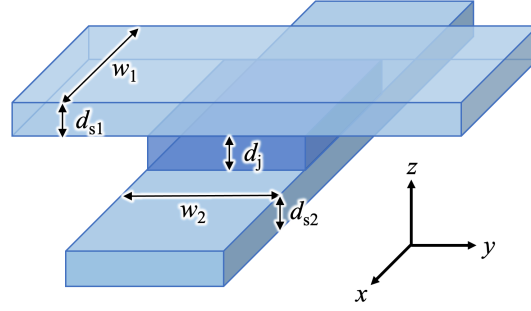


Figure 2. Schematic of a cross-type Josephson junction with two superconducting nanostrips. The barrier layer is located at $|x| < w_1/2$, $|y| < w_2/2$, and $|z| < d_j/2$. The top superconducting strip is located at $|x| < w_1/2$, $|y| < \infty$, and $d_j/2 < z < d_{s1} + d_j/2$, where $d_{s1} < \lambda$ and $w_1 < \lambda^2/d_{s1}$. The bottom superconducting strip is located at $|x| < \infty$, $|y| < w_2/2$, and $-d_{s2} - d_j/2 < z < -d_j/2$, where $d_{s2} < \lambda$ and $w_2 < \lambda^2/d_{s2}$.

integrating the London equation, $\nabla \times \mathbf{J} = -\mathbf{B}/\mu_0\lambda^2 \simeq -\mathbf{H}/\lambda^2$, where $\mathbf{H} = (H_x, H_y, H_z)$ is the applied uniform magnetic field. The screening current density \mathbf{J}_1 in the top strip and \mathbf{J}_2 in the bottom strip are thus given by

$$\mathbf{J}_1 = \frac{1}{\lambda^2} \left[-xH_z\hat{\mathbf{y}} + \left(z - \frac{d_{s1} + d_j}{2} \right) (-H_y\hat{\mathbf{x}} + H_x\hat{\mathbf{y}}) \right], \quad (7)$$

$$\mathbf{J}_2 = \frac{1}{\lambda^2} \left[yH_z\hat{\mathbf{x}} + \left(z + \frac{d_{s2} + d_j}{2} \right) (-H_y\hat{\mathbf{x}} + H_x\hat{\mathbf{y}}) \right]. \quad (8)$$

Substitution of equations (7) and (8) into equations (5) and (6) yields

$$\frac{\phi_0}{2\pi\mu_0} \frac{\partial\theta(x, y)}{\partial x} = d_{\text{eff}}H_y - yH_z, \quad (9)$$

$$\frac{\phi_0}{2\pi\mu_0} \frac{\partial\theta(x, y)}{\partial y} = -d_{\text{eff}}H_x - xH_z, \quad (10)$$

where d_{eff} is the effective junction thickness for thin superconducting films as follows [27]

$$d_{\text{eff}} = d_j + (d_{s1} + d_{s2})/2. \quad (11)$$

Integrating equations (9) and (10), we obtain the resulting distribution of the gauge-invariant phase difference,

$$\theta(x, y) = \theta_0 + \frac{2\pi\mu_0}{\phi_0} \left[d_{\text{eff}}(xH_y - yH_x) - xyH_z \right], \quad (12)$$

where θ_0 is the integral constant. Note that θ is given as the sum of the parallel-field contribution ($\propto xH_y - yH_x$) and the perpendicular-field contribution ($\propto xyH_z$) [7], and the simple formula of equation (12) is obtained for weak magnetic screening.

Responding to the perpendicular field H_z , the screening current flowing in superconducting strips produces an effective parallel magnetic field in the junctions [7], resulting in a modulation of θ . Thus, the perpendicular field H_z modulates θ through J_x and J_y , as shown in the right-hand sides of equations (5) and (6).

3. dc critical currents of cross-type Josephson junctions

3.1. General expression for critical currents

The Josephson current density across the junction is $J_z = J_c \sin \theta$, where J_c is the critical current density. The net current I_z across the junction is given by

$$I_z = \int_{-w_1/2}^{w_1/2} dx \int_{-w_2/2}^{w_2/2} dy J_c \sin[\theta(x, y)] = J_c \text{Im} \int_{-w_1/2}^{w_1/2} dx \int_{-w_2/2}^{w_2/2} dy \exp\{i[\theta_0 + \theta_1(x, y)]\}, \quad (13)$$

where equation (12) is rewritten as $\theta(x, y) = \theta_0 + \theta_1(x, y)$ and

$$\theta_1(x, y) = \frac{2x}{w_1}\beta - \frac{2y}{w_2}\alpha - \frac{4xy}{w_1w_2}\gamma. \quad (14)$$

The parameters α , β , and γ in equation (14) are defined by

$$\alpha = \pi\Phi_x/\phi_0, \quad \Phi_x = \mu_0 H_x w_2 d_{\text{eff}}, \quad (15)$$

$$\beta = \pi\Phi_y/\phi_0, \quad \Phi_y = \mu_0 H_y w_1 d_{\text{eff}}, \quad (16)$$

$$\gamma = \pi\Phi_z/2\phi_0, \quad \Phi_z = \mu_0 H_z w_1 w_2, \quad (17)$$

where $\Phi_x = \mu_0 H_x S_x$, $\Phi_y = \mu_0 H_y S_y$, and $\Phi_z = \mu_0 H_z S_z$ are the magnetic fluxes linked in the areas $S_x = w_2 d_{\text{eff}}$, $S_y = w_1 d_{\text{eff}}$, and $S_z = w_1 w_2$, respectively.

The dc critical current I_c is obtained by maximizing I_z with respect to θ_0 . Equation (13) is rewritten in the form $I_z = \text{Im}[f \exp(i\theta_0)]$, which has a maximum of $|f|$. We thus obtain $I_c = J_c \int dx \int dy \exp(i\theta_1)$ [3]. That is,

$$\frac{I_c(\Phi_x, \Phi_y, \Phi_z)}{I_{c0}} = \left| \mathcal{I} \left(\frac{\pi\Phi_x}{\phi_0}, \frac{\pi\Phi_y}{\phi_0}, \frac{\pi\Phi_z}{2\phi_0} \right) \right|, \quad (18)$$

where I_{c0} is the critical current at zero magnetic field,

$$I_{c0} = I_c(0, 0, 0) = J_c w_1 w_2, \quad (19)$$

and the complex-valued function $\mathcal{I}(\alpha, \beta, \gamma)$ is defined by

$$\mathcal{I}(\alpha, \beta, \gamma) = \frac{1}{4} \int_{-1}^1 dx' \int_{-1}^1 dy' \exp[i(\alpha y' + \beta x' + \gamma x' y')]. \quad (20)$$

The integral variables in equation (20) are $x' = 2x/w_1$ and $y' = -2y/w_2$. See Appendix A for details on $\mathcal{I}(\alpha, \beta, \gamma)$. The symmetry in $\mathcal{I}(\alpha, \beta, \gamma)$ shown in equation (A.1) leads to symmetry in the critical current $I_c \propto |\mathcal{I}|$,

$$I_c(-\Phi_x, \Phi_y, \Phi_z) = I_c(\Phi_x, -\Phi_y, \Phi_z) = I_c(\Phi_x, \Phi_y, -\Phi_z) = I_c(\Phi_x, \Phi_y, \Phi_z). \quad (21)$$

We thus consider only the case when $\Phi_x \geq 0$, $\Phi_y \geq 0$, and $\Phi_z \geq 0$.

3.2. Critical currents in parallel or perpendicular fields

The I_c for parallel magnetic fields (i.e., $\Phi_z = 0$) is obtained from equation (A.2), and is given by

$$\frac{I_c(\Phi_x, \Phi_y, 0)}{I_{c0}} = \left| \frac{\sin(\pi\Phi_x/\phi_0) \sin(\pi\Phi_y/\phi_0)}{\pi\Phi_x/\phi_0 \pi\Phi_y/\phi_0} \right|, \quad (22)$$

which shows the standard Fraunhofer-like interference [4].

The I_c for perpendicular magnetic fields (i.e., $\Phi_x = \Phi_y = 0$) is obtained from equation (A.3), and is given by [7]

$$\frac{I_c(0, 0, \Phi_z)}{I_{c0}} = \frac{\text{Si}(\pi\Phi_z/2\phi_0)}{\pi\Phi_z/2\phi_0}, \quad (23)$$

where $\text{Si}(z) = \int_0^z dt(\sin t)/t$ is the sine integral [29]. Note that $I_c(0, 0, \Phi_z)$ monotonically decreases with increasing Φ_z and shows no interference patterns [7]. The contribution of the phase difference θ from the perpendicular field H_z is proportional to H_z , as shown in equation (12), and the modulation of θ due to H_z results in the decrease of the critical currents as $I_c \sim 1/H_z$ for large H_z [7, 24].

3.3. Critical currents in two-dimensional oblique fields

The I_c for $\Phi_y = 0$ is obtained from equation (A.4), and is given by

$$\frac{I_c(\Phi_x, 0, \Phi_z)}{I_{c0}} = \left| \frac{\text{Si}[\pi(\Phi_x + \Phi_z/2)/\phi_0] - \text{Si}[\pi(\Phi_x - \Phi_z/2)/\phi_0]}{\pi\Phi_z/\phi_0} \right|. \quad (24)$$

For $\Phi_x = \Phi_z/2$ and $\Phi_y = 0$ we have $I_c(\Phi_z/2, 0, \Phi_z) = I_c(0, 0, 2\Phi_z)$.

Figures 3 and 4 show the plots of I_c vs Φ_x and I_c vs Φ_z , respectively, where I_c is obtained from equation (24). The plot of I_c vs Φ_x for $\Phi_z = 0$ in figure 3(a) corresponds to the Fraunhofer-like interference pattern given by equation (22) for $\Phi_y = 0$. The plot of I_c vs Φ_z for $\Phi_x = 0$ in figure 4(a) shows the monotonic dependence given by equation (23). Interference patterns appear when $|\Phi_z| < 2|\Phi_x|$. As shown in Figs. 3(a) and 4(a), the I_c for $\Phi_z < 2\Phi_x$ is much smaller than I_{c0} when $\Phi_x/\phi_0 \approx 1, 2, 3, 4, \dots$ and $\Phi_z/\phi_0 \approx 0, 1, 3, 5, \dots$. As shown in Figs. 3(b) and 4(b), the I_c for $\Phi_z < 2\Phi_x$ is much smaller than I_{c0} also when $\Phi_x/\phi_0 \approx 3/2, 5/2, 7/2, 9/2, \dots$ and $\Phi_z/\phi_0 \approx 2, 4, 6, 8, \dots$. The I_c with the magnetic interference is generally suppressed for $|\Phi_z| < 2|\Phi_x|$, while the I_c without the magnetic interference is relatively large for $|\Phi_z| > 2|\Phi_x|$. Therefore, the I_c temporarily increases with Φ_z at $|\Phi_z| \sim 2|\Phi_x|$, as seen in Fig. 4.

Figure 5 shows density plots of I_c as a function of (Φ_x, Φ_z) . For $|\Phi_z| < 2|\Phi_x|$ [i.e., the right-lower region below the dashed line in the (Φ_x, Φ_z) plane], the stepwise dark lines corresponding to $I_c \ll I_{c0}$ clearly demonstrate the interference patterns of $I_c(\Phi_x, 0, \Phi_z)$, which are consistent with the behavior shown in Figs. 3 and 4.

Substitution of $\alpha = (n + 1/2)\pi$ or $\gamma = (m + 1/2)\pi$ (where n and m are integers) in equation (A.5) yields

$$\frac{I_c(\Phi_x, 0, \Phi_z)}{I_{c0}} \sim \left| \frac{\sin(\pi\Phi_x/\phi_0)}{\pi\Phi_x/\phi_0} \frac{\sin(\pi\Phi_z/2\phi_0)}{\pi\Phi_z/2\phi_0} \right| \quad (25)$$

for $\Phi_x/\phi_0 = n + 1/2$ or $\Phi_z/\phi_0 = 2m + 1$. Equation (25) roughly explains the interference patterns shown in Figs. 3(a) and

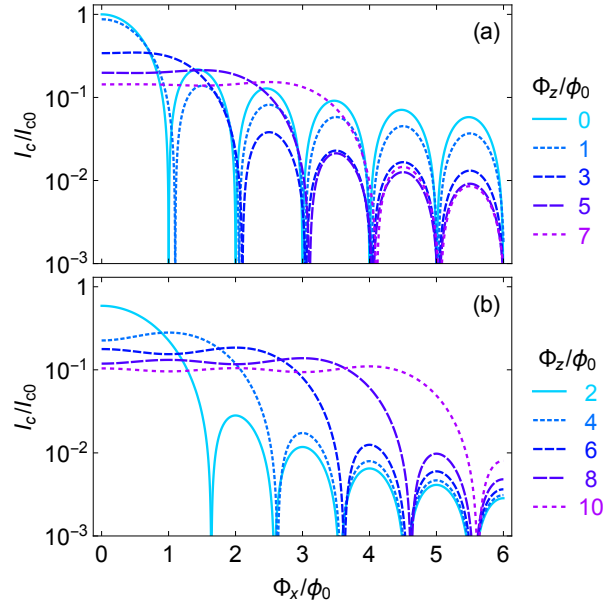


Figure 3. Critical current $I_c(\Phi_x, 0, \Phi_z)/I_{c0}$ vs parallel magnetic flux $\alpha/\pi = \Phi_x/\phi_0$ for (a) $2\gamma/\pi = \Phi_z/\phi_0 = 0, 1, 3, 5,$ and 7 , and (b) $\Phi_z/\phi_0 = 2, 4, 6, 8,$ and 10 .

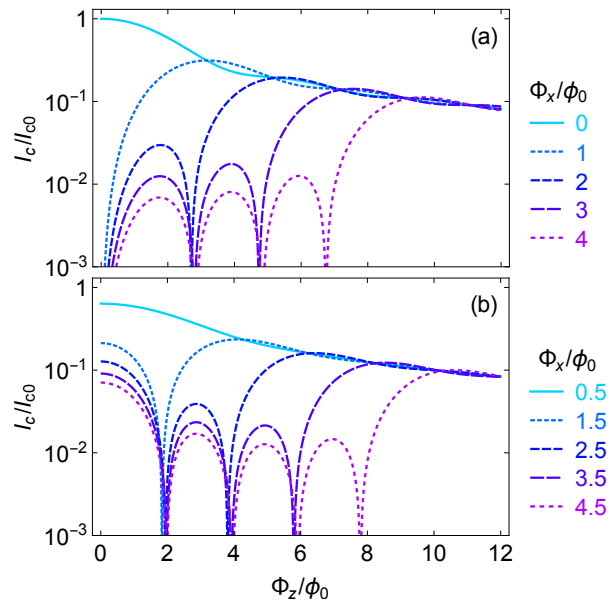


Figure 4. Critical current $I_c(\Phi_x, 0, \Phi_z)/I_{c0}$ vs perpendicular magnetic flux $2\gamma/\pi = \Phi_z/\phi_0$ for (a) $\alpha/\pi = \Phi_x/\phi_0 = 0, 1, 2, 3,$ and 4 , and (b) $\Phi_x/\phi_0 = 1/2, 3/2, 5/2, 7/2,$ and $9/2$.

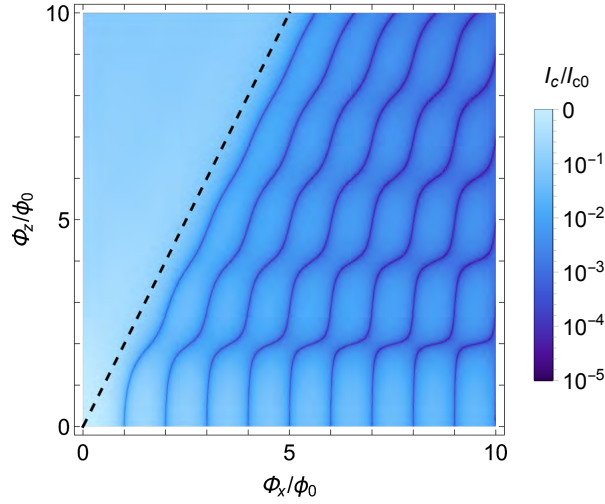


Figure 5. Logarithmic density plot of the critical current $I_c(\Phi_x, 0, \Phi_z)/I_{c0}$ as a function of the parallel $\alpha/\pi = \Phi_x/\phi_0$ and perpendicular magnetic flux $2\gamma/\pi = \Phi_z/\phi_0$. The dashed line corresponds to $\Phi_z = 2\Phi_x$.

4(b). Substitution of $\alpha = n\pi$ or $\gamma = m\pi$ (where n and m are integers) into equation (A.5) yields

$$\frac{I_c(\Phi_x, 0, \Phi_z)}{I_{c0}} \sim \left| \frac{\cos(\pi\Phi_x/\phi_0)}{(\pi\Phi_x/\phi_0)^2} \cos(\pi\Phi_z/2\phi_0) \right| \quad (26)$$

for $\Phi_x/\phi_0 = n$ or $\Phi_z/\phi_0 = 2m$. Equation (26) roughly reproduces the interference patterns shown in Figs. 3(b) and 4(a). Equation (A.6) yields

$$\frac{I_c(\Phi_x, 0, \Phi_z)}{I_{c0}} \sim \left| \frac{\phi_0}{\Phi_z} - \cos(\pi\Phi_x/\phi_0) \frac{\cos(\pi\Phi_z/2\phi_0)}{(\pi\Phi_z/2\phi_0)^2} \right|, \quad (27)$$

which roughly explains the behavior of I_c without interference shown in Figs. 3 and 4.

3.4. Critical currents in three-dimensional oblique fields

Figure 6 shows density plots of I_c as a function of (Φ_x, Φ_y) . The interference patterns of I_c disappear in the bright regions of $|\Phi_z| > 2 \max(|\Phi_x|, |\Phi_y|)$. Dark lines or spots corresponding to the case where $I_c \ll I_{c0}$ show peculiar interference patterns with horizontal and vertical checkerboard patterns seen for integer Φ_z/ϕ_0 (upper panels of figure 6) and diagonal checkerboard patterns seen for half-integer Φ_z/ϕ_0 (lower panels of figure 6). These patterns are roughly reproduced by the simplified expression in equation (A.13).

Figure 7 shows the density plots of I_c as a function of $(\Phi_{\parallel}, \Phi_z)$, where $\Phi_{\parallel} \equiv (\Phi_x^2 + \Phi_y^2)^{1/2}$. The parameter $\vartheta \equiv \arctan(\Phi_y/\Phi_x) = \arctan[(w_1/w_2)(H_y/H_x)]$ corresponds to the field angle in the xy plane when $w_1 = w_2$. If we simply denote the ϑ dependence of the critical current as $I_c(\vartheta)$, the $I_c(\vartheta)$ has a periodicity expressed as $I_c(\pi/2 + \vartheta) = I_c(\pi/2 - \vartheta) = I_c(\vartheta)$, as seen in Fig. 6. The $I_c(\vartheta)$ for $0 < \vartheta \leq \pi/4$ is plotted in Fig. 7. Noticeable I_c -interference texture like weaving patterns, which can also be reproduced by equation (A.13), are seen in the region of $\Phi_z < 2\Phi_{\parallel} \min(\cos \vartheta, \sin \vartheta)$.

4. Discussion and summary

We considered the response of sandwich-type Josephson junctions in three-dimensional magnetic fields $\mathbf{H} = (H_x, H_y, H_z)$. It should be noted that the response to the perpendicular field H_z is much more sensitive than that to the parallel magnetic field H_{\parallel} if the junction dimensions in the xy plane are much larger than the effective junction thickness $w_j \gg d_{\text{eff}}$, where $H_{\parallel} \equiv (H_x^2 + H_y^2)^{1/2}$ and $w_j \equiv \min(w_1, w_2)$. Even when $|H_z| \sim H_{\parallel}$, we have $|\Phi_z/\Phi_{\parallel}| \geq |H_z/H_{\parallel}|(w_j/d_{\text{eff}}) \gg 1$ from equations (15)–(17). Therefore, when the dependence of I_c on the field angle from the xy plane $\vartheta_H = \arctan(H_z/H_{\parallel})$ is investigated, the theoretical results presented in this paper may be observed in the narrow angle range of $|\vartheta_H| < d_{\text{eff}}/w_j \ll 1$. The present theory considers the case where the applied magnetic field is smaller than the lower critical field and no vortices are present in the junctions. In perpendicular geometry, vortices are easily to penetrate into the junctions, and the perpendicular field H_z should be small enough.

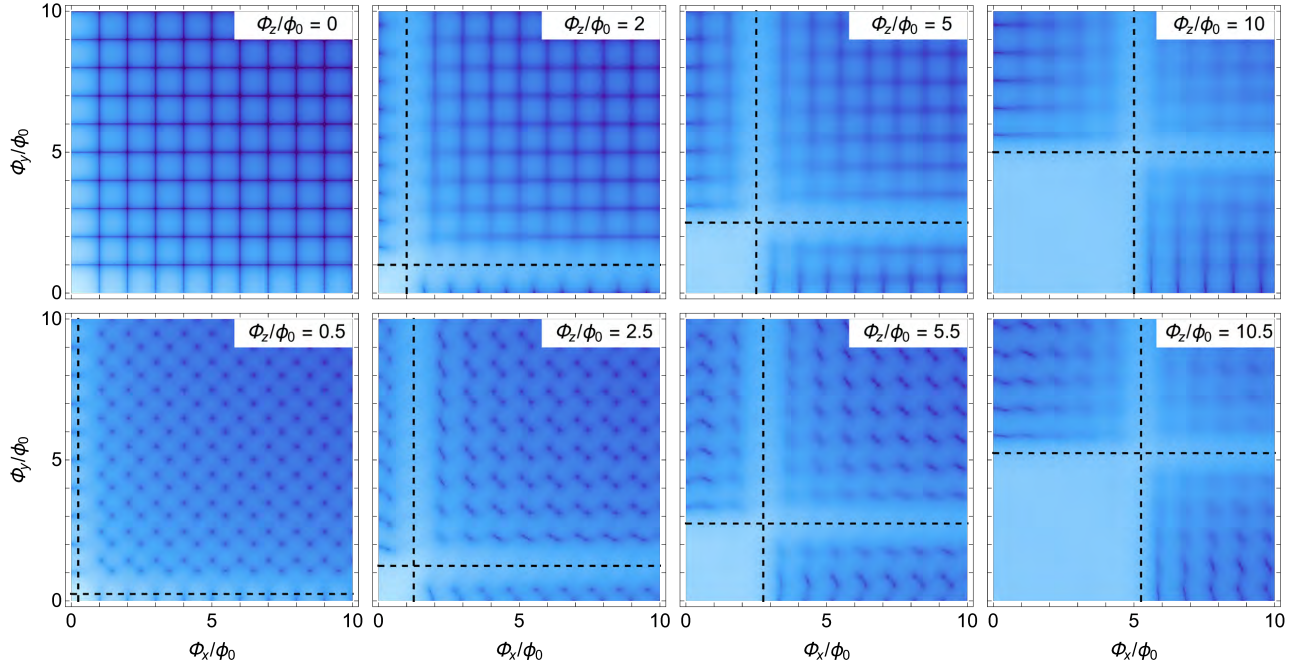


Figure 6. Logarithmic density plots of the critical current $I_c(\Phi_x, \Phi_y, \Phi_z)/I_{c0}$ as a function of $\alpha/\pi = \Phi_x/\phi_0$ and $\beta/\pi = \Phi_y/\phi_0$ when $2\gamma/\pi = \Phi_z/\phi_0$ is integer (upper panels) and half integer (lower panels). The color scale in these plots is the same as in figure 5. Vertical and horizontal dashed lines correspond to $\Phi_z = 2\Phi_x$ and $\Phi_z = 2\Phi_y$, respectively.

The junction geometry and configuration of the superconducting films affect the interference behavior of I_c . The I_c for overlap-type junctions in perpendicular fields H_z show Fraunhofer-type interference patterns [22, 23], whereas I_c for cross-type junctions monotonically decrease with H_z without interference [7]. Monaco *et al.* [24] numerically showed that interference patterns in I_c vs H_z strongly depend on the configuration of the superconducting strips. Although we consider only cross-type junctions in this paper, the I_c interference in oblique fields for other geometries (e.g., overlap-type junctions) is expected to show different patterns from our results.

In this paper we assume that the critical current density J_c is homogeneous in the Josephson junctions, although inhomogeneous J_c affects the interference patterns of I_c [4, 6]. The inhomogeneous current distributions arising from the edge states in topological insulators [18, 19, 20] and in graphene [21] are investigated by analyzing the interference patterns of I_c . It would be interesting to consider the effects of the inhomogeneous $J_c(x, y)$ due to the edge states in topological materials upon the interference patterns of the sandwich-type junctions in three-dimensional magnetic fields.

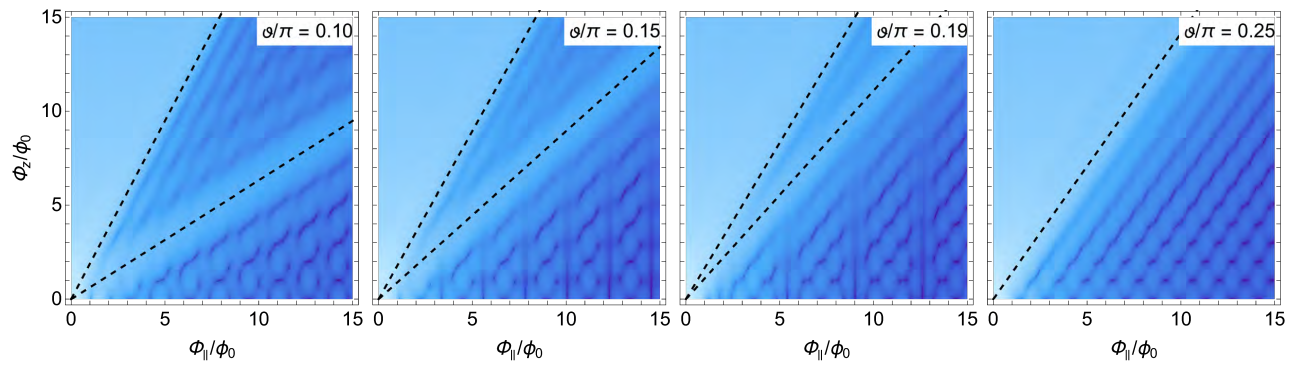


Figure 7. Logarithmic density plots of the critical current $I_c(\Phi_{\parallel} \cos \vartheta, \Phi_{\parallel} \sin \vartheta, \Phi_z)/I_{c0}$ as a function of $\Phi_{\parallel} \equiv (\Phi_x^2 + \Phi_y^2)^{1/2}$ and Φ_z for $\vartheta \equiv \arctan(\Phi_y/\Phi_x) = 0.10\pi, 0.15\pi, 0.19\pi,$ and 0.25π . The color scale in these plots is the same as in figure 5. Upper and lower dashed lines correspond to $\Phi_z = 2\Phi_x = 2\Phi_{\parallel} \cos \vartheta$ and $\Phi_z = 2\Phi_y = 2\Phi_{\parallel} \sin \vartheta$, respectively.

To summarize, we theoretically investigate the dc critical current I_c of cross-type Josephson junctions with thin and narrow superconducting strips exposed to three-dimensional magnetic fields (Φ_x, Φ_y, Φ_z) for weak magnetic screening in the junctions and in the strips. The standard Fraunhofer-type magnetic interference for parallel magnetic fields is strongly modulated by the perpendicular field, and the magnetic interference disappears when $|\Phi_z| > 2 \max(|\Phi_x|, |\Phi_y|)$. Phase manipulation by the perpendicular field results in a variety of the magnetic interference of I_c , and might be useful for developing novel Josephson-junction devices.

Acknowledgments

I thank E. S. Otabe, T. Ueda, Y. Higashi, H. Asai, Y. Yamanashi, I. Kakeya, and M. Hidaka for stimulating discussions. This work has been supported by JSPS KAKENHI JP20K05314.

Appendix A. The complex-valued function $I(\alpha, \beta, \gamma)$

We now present the mathematical formulae for the complex-valued critical current $I(\alpha, \beta, \gamma)$ defined by equation (20). Because of the following symmetries, we need only consider the case when $\alpha \geq 0, \beta > 0$, and $\gamma > 0$:

$$I(-\alpha, \beta, \gamma) = I(\alpha, -\beta, \gamma) = I(\alpha, \beta, -\gamma) = I^*(\alpha, \beta, \gamma), \quad (\text{A.1})$$

where I^* is the complex conjugate of I .

The I for $\gamma = 0$ and for $\alpha = \beta = 0$ are respectively given by

$$I(\alpha, \beta, 0) = (\sin \alpha \sin \beta) / \alpha \beta, \quad (\text{A.2})$$

$$I(0, 0, \gamma) = \text{Si}(\gamma) / \gamma. \quad (\text{A.3})$$

The I for $\beta = 0$ is

$$I(\alpha, 0, \gamma) = \frac{1}{2\gamma} [\text{Si}(\alpha + \gamma) - \text{Si}(\alpha - \gamma)]. \quad (\text{A.4})$$

The asymptotic behavior of equation (A.4) for $|\alpha| \gg |\gamma|$ is

$$I(\alpha, 0, \gamma) \sim \frac{\sin \alpha \sin \gamma}{\alpha \gamma} + \frac{\cos \alpha}{\alpha^2} \left(\cos \gamma - \frac{\sin \gamma}{\gamma} \right), \quad (\text{A.5})$$

and that for $|\alpha| \ll |\gamma|$ is

$$I(\alpha, 0, \gamma) \sim \frac{\pi}{2\gamma} - \cos \alpha \frac{\cos \gamma}{\gamma^2}. \quad (\text{A.6})$$

Equation (20) is generally rewritten as

$$I(\alpha, \beta, \gamma) = \frac{ie^{-i\alpha\beta/\gamma}}{4\gamma} \left[F(\eta_1) - F(\eta_2) - F(\eta_3) + F(\eta_4) \right], \quad (\text{A.7})$$

where

$$\eta_1 = (\alpha + \gamma)(\beta + \gamma) / \gamma, \quad (\text{A.8})$$

$$\eta_2 = (\alpha - \gamma)(\beta + \gamma) / \gamma, \quad (\text{A.9})$$

$$\eta_3 = (\alpha + \gamma)(\beta - \gamma) / \gamma, \quad (\text{A.10})$$

$$\eta_4 = (\alpha - \gamma)(\beta - \gamma) / \gamma. \quad (\text{A.11})$$

The complex-valued function $F(z)$ in equation (A.7) is defined by

$$F(z) = \int_0^z \frac{1 - e^{it}}{t} dt = -i \text{Si}(z) - \text{Ci}(z) + \mathbf{C} + \ln z, \quad (\text{A.12})$$

where $\text{Ci}(z) = -\int_z^\infty dt (\cos t) / t$ is the cosine integral and $\mathbf{C} = 0.577\dots$ is Euler's constant [29]. The general asymptotic behavior of equation (A.7) for small γ [i.e., for $\max(|\alpha|, |\beta|) \gg |\gamma|$] is

$$I(\alpha, \beta, \gamma) \sim \frac{1}{\alpha\beta} (\sin \alpha \sin \beta \cos \gamma - i \cos \alpha \cos \beta \sin \gamma), \quad (\text{A.13})$$

and that for large γ [i.e., for $\max(|\alpha|, |\beta|) \ll |\gamma|$] is

$$I(\alpha, \beta, \gamma) \sim \frac{\pi}{2\gamma} - \frac{i\pi\alpha\beta}{2\gamma^2} - \frac{e^{i\alpha\beta/\gamma}}{\gamma^2} (\cos \alpha \cos \beta \cos \gamma - i \sin \alpha \sin \beta \sin \gamma). \quad (\text{A.14})$$

References

- [1] Rowell J M 1963 Magnetic Field Dependence of the Josephson Tunnel Current *Phys. Rev. Lett.* **11** 200
- [2] Jaklevic R C, Lambe J, Silver A H and Mercereau J E 1964 Quantum Interference Effects in Josephson Tunneling *Phys. Rev. Lett.* **12** 159
- [3] Josephson B D 1965 Supercurrents through barriers *Adv. Phys.* **14** 419
- [4] Barone A and Paterno G 1982 *Physics and Applications of the Josephson Effect* (New York: Wiley).
- [5] Clarke J, Braginski A I, eds. 2004 *The SQUID handbook* (Wiley).
- [6] Dynes R C and Fulton T A 1971 Supercurrent Density Distribution in Josephson Junctions *Phys. Rev. B* **3** 3015
- [7] Miller S, Biagi K, Clem J and Finnemore D 1985 Critical currents of cross-type superconducting-normal-superconducting junctions in perpendicular magnetic fields *Phys. Rev. B* **31** 2684
- [8] Gubankov V N, Lisitskii M P, Serpuchenko I L and Fistul M V 1991 Effect of Abrikosov vortices on the critical current of a Josephson junction *Sov. Phys. JETP* **73** 734
- [9] Golod T, Rydh A and Krasnov V M 2010 Detection of the Phase Shift from a Single Abrikosov Vortex *Phys. Rev. Lett.* **104** 227003
- [10] Clem J R 2011 Effect of nearby Pearl vortices upon the I_c versus B characteristics of planar Josephson junctions in thin and narrow superconducting strips *Phys. Rev. B* **84** 134502
- [11] Nappi C, Lissitski M P and Cristiano R 2002 Fraunhofer critical-current diffraction pattern in annular Josephson junctions with injected current *Phys. Rev. B* **65** 132516
- [12] Goldobin E, Sterck A, Gaber T, Koelle D and Kleiner R 2004 Dynamics of Semifluxons in Nb Long Josephson $0-\pi$ Junctions *Phys. Rev. Lett.* **92** 057005
- [13] Kogan V G and Mints R G 2014 Effect of current injection into thin-film Josephson junctions *Phys. Rev. B* **90** 184504
- [14] Kemmler M, Weides M, Weiler M, Opel M, Goennenwein S T B, Vasenko A S, Golubov A A, Kohlstedt H, Koelle D, Kleiner R and Goldobin E 2010 Magnetic interference patterns in $0-\pi$ superconductor/insulator/ferromagnet/superconductor Josephson junctions: Effects of asymmetry between 0 and π regions *Phys. Rev. B* **81** 054522
- [15] Alidoust M, Sewell G and Linder J 2012 Non-Fraunhofer Interference Pattern in Inhomogeneous Ferromagnetic Josephson Junctions *Phys. Rev. Lett.* **108** 037001
- [16] Börcsök B, Komori S, Buzdin A I and Robinson J W A 2019 Fraunhofer patterns in magnetic Josephson junctions with non-uniform magnetic susceptibility *Sci. Rep.* **9** 5616
- [17] Suominen H J, Danon J, Kjaergaard M, Flensberg K, Shabani J, Palmstrøm C J, Nichele F and Marcus C M 2017 Anomalous Fraunhofer interference in epitaxial superconductor-semiconductor Josephson junctions *Phys. Rev. B* **95** 035307
- [18] Lee J H, Lee G-H, Park J, Lee J, Nam S-G, Shin Y-S, Kim J S and Lee H-J 2014 Local and Nonlocal Fraunhofer-like Pattern from an Edge-Stepped Topological Surface Josephson Current Distribution *Nano Lett.* **14** 5029
- [19] Hart S, Ren H, Wagner T, Leubner P, Mühlbauer M, Brüne C, Buhmann H, Molenkamp L W and Yacoby A 2014 Induced superconductivity in the quantum spin Hall edge *Nature Phys.* **10** 638
- [20] Pribiag V S, Beukman A J A, Qu F, Cassidy M C, Charpentier C, Wegscheider W and Kouwenhoven L P 2015 Edge-mode superconductivity in a two-dimensional topological insulator *Nature Nanotech* **10** 593
- [21] Allen M T, Shtanko O, Fulga I C, Akhmerov A R, Watanabe K, Taniguchi T, Jarillo-Herrero P, Levitov L S and Yacoby A 2016 Spatially resolved edge currents and guided-wave electronic states in graphene *Nature Phys.* **12** 128
- [22] Rosenstein I and Chen J T 1975 Effect of Transverse Magnetic Fields on dc Josephson Current *Phys. Rev. Lett.* **35** 303
- [23] Hebard A F and Fulton T A 1975 Josephson Junctions in Transverse Magnetic Fields *Phys. Rev. Lett.* **35** 1310
- [24] Monaco R, Aaroe M, Mygind J and Koshelets V P 2008 Static properties of small Josephson tunnel junctions in a transverse magnetic field *J. Appl. Phys.* **104** 023906
- [25] Watanabe N, Nakayama A, Abe S and Aizawa K 2005 Magnetic field dependence of Josephson current by applying the external magnetic field perpendicular to the Josephson junction *J. Appl. Phys.* **97** 10B116
- [26] Anderson P W and Rowell J M 1963 Probable Observation of the Josephson Superconducting Tunneling Effect *Phys. Rev. Lett.* **10** 230
- [27] Weihnacht M 1969 Influence of Film Thickness on D. C. Josephson Current *Phys. Stat. Sol. (b)* **32** K169
- [28] Gurevich A 1992 Nonlocal Josephson electrostatics and pinning in superconductors *Phys. Rev. B* **46** 3187
- [29] Gradshteyn I S and I. M. Ryshik I M 1994 *Table of Integrals, Series, and Products*, 5th ed. (London: Academic)